Journal of Environmental Chemical Engineering 10 (2022) 107441

Contents lists available at ScienceDirect

Journal of Environmental Chemical Engineering

journal homepage: www.elsevier.com/locate/jece

Efficient photoelectrochemical conversion of CO_2 to ethylene and methanol using a Cu cathode and TiO_2 nanoparticles synthesized in supercritical medium as photoanode

Ivan Merino-Garcia [a,*,1], Sergio Castro [a,1], Angel Irabien [a], Ignacio Hernández [b], Verónica Rodríguez [c], Rafael Camarillo [c], Jesusa Rincón [c], Jonathan Albo [a,*]

[a] Departamento de Ingenierías Química y Biomolecular, Universidad de Cantabria, Avda. Los Castros, s/n, 39005 Santander, Spain
[b] Departamento CITIMAC, Universidad de Cantabria, Avda. Los Castros, s/n, 39005 Santander, Spain
[c] Department of Chemical Engineering, Faculty of Environmental Sciences and Biochemistry, Universidad de Castilla-La Mancha, Avda. Carlos III, s/n, 45071 Toledo, Spain

ARTICLE INFO

Editor: Vítor J.P. Vilar

Keywords:
Photoelectrocatalysis
Continuous CO_2 conversion
Photoanode-driven system
TiO_2 in supercritical medium
Ethylene
Methanol

ABSTRACT

The photoelectrochemical conversion of CO_2 into valuable products represents an attractive method to decrease the external electrical bias required in electrochemical approaches. In this work, TiO_2 nanoparticles with enhanced optical properties, large surface area, appropriate morphology, and superior crystallinity are synthesized in supercritical medium to manufacture light-responsive photoanodes. The photoelectrochemical CO_2 reduction tests are carried out in continuous mode using a photoanode-driven filter-press cell illuminated with UV LED lights (100 mW cm^{-2}), consisting on TiO_2 nanoparticles synthesized in supercritical medium (3 mg cm^{-2}) supported onto porous carbon paper as the photoanode, a Cu plate cathode, and 1 M KOH aqueous solution as the reaction medium. The main products obtained from CO_2 are ethylene in the gas phase, together with methanol in the liquid phase. The results show that reaction performance is improved under UV irradiation towards ethylene ($r = 147.4$ μmol m^{-2} s^{-1}; $FE = 46.6\%$) and methanol ($r = 4.72$ μmol m^{-2} s^{-1}; $FE = 15.3\%$) in comparison with the system performance in the dark (ethylene: $r = 24.2$ μmol m^{-2} s^{-1} and $FE = 38.2\%$; methanol not detected), which can be mainly ascribed to the superior photocurrent densities reached that affect the selectivity of the reaction. Besides, the maximum solar-to-fuels values achieved for ethylene (5.4%) and methanol (1.9%) are markedly superior to those observed with illuminated TiO_2-P25 photoanodes under the same reactor configuration and experimental conditions (3.7% and 1%, respectively). Therefore, these results demonstrate the benefits of using TiO_2-based materials synthesized in supercritical medium for a more efficient continuous photoelectroreduction of CO_2 to value-added products.

1. Introduction

The intensification of human industrial activities is causing an unbalanced CO_2 produced and consumed on Earth [1,2]. Among the available sustainable possibilities to accelerate an energy transition away from fossil fuels, the chemical conversion of CO_2 and water into valuable products represents a promising direction to equilibrate the system and close the carbon cycle [3–5]. Several approaches can be considered to meet the target, namely mineralization [6], enzymatic [7], thermochemical [8], electrochemical [9,10], photoelectrochemical (PEC) [11–13], and photochemical processes [14,15]. In particular, the transformation of CO_2 via PEC provides greener CO_2 utilization routes towards the generation of fuels and chemicals under light irradiation, integrating the benefits of both electrocatalytic and photocatalytic conversion approaches, and promoting the separation efficiency of photogenerated electron-hole pairs [12,16–19]. Besides, the production of ethylene (C_2H_4) from CO_2 utilization is interesting, since this hydrocarbon represents an energy-dense chemical feedstock used in several applications as energy vector and chemical building blocks [20,21]. The production of alcohols such as methanol (CH_3OH) is also of

* Corresponding authors.
E-mail addresses: merinoi@unican.es (I. Merino-Garcia), alboj@unican.es (J. Albo).
[1] I. Merino-Garcia and S. Castro contributed equally to this work as first authors.

https://doi.org/10.1016/j.jece.2022.107441
Received 8 November 2021; Received in revised form 17 January 2022; Accepted 18 February 2022
Available online 22 February 2022
2213-3437/

utmost importance, owing to its key role in several applications, namely as a chemical storage carrier for hydrogen or as a platform product in gasoline and biodiesel [22–24].

Depending on the nature of the (photo)electrodes used in two-compartment PEC cells, four different photoreactor configurations can be applied: i) photoanode/dark cathode [25–27], ii) dark anode/photocathode [28], iii) photoanode/photocathode [29,30], and iv) hybrid PEC-solar cell tandem [31]. The first PEC configuration is simpler and usually preferred to improve the energy efficiency of the process since the photoanode provides extra photogenerated electrons from water oxidation to the cathode compartment for CO_2 reduction, decreasing the requirements of external electrical energy [31]. Thus, photoanode-driven PEC processes can lead to decreased cell bias, which makes this strategy the most suitable option from energy efficiency and practical application viewpoints [32–34].

Although a wide variety of photoactive materials can be seen in PEC systems as photoanodes, such as WO_3, $BiVO_4$, Fe_2O_3, or ZnO [31,35–40], among others, TiO_2-P25 has been the most investigated light-responsive material in photoanode-driven PEC systems, owing to its low cost, non-toxic characteristics, photo-stability, wide bandgap (> 3.0 eV), chemical inertness, large resistance to photo-corrosion, and UV light absorption properties [36,41,42]. Nevertheless, TiO_2-P25 presents several limitations [31,43], mainly: i) fast recombination of electron-hole pairs and ii) low purity and crystallinity. In this respect, different morphologies (e.g., nanotubes, nanospheres) of TiO_2 have been recently investigated to improve electron mobility, chemical stability, and surface area, among others [18,44]. Moreover, the modification of these structures (i.e., titania nanotubes) with noble metal particles such as Au and Ag has also been proposed to decrease the photogenerated carrier recombination efficiency of TiO_2 [18,45], which should allow for achieving a higher photoelectrochemical conversion performance. On the other hand, alternative synthesis methods have been proposed to overcome the main shortcomings of benchmark TiO_2 [46,47]. Among them, the preparation of TiO_2 in supercritical medium led to improved photocatalytic properties compared to those prepared under conventional procedures [47–50]. Specifically, several properties such as surface area, light absorption, optical bandgap energy, presence of surface hydroxyl groups, and appropriate morphology (for enhanced charge separation) are improved in comparison with commercial TiO_2-P25 [43].

Previous studies in our group reported the preparation, characterization, and use of commercial TiO_2-P25 nanoparticulated electrodes as light-responsive photoanodes in a continuous photoanode-driven PEC process illuminated with UV LED lights. A Cu plate was utilized as a dark cathode to reduce CO_2 in a filter-press PEC cell divided by a Nafion® 117 membrane [25]. The energy requirements to carry out the CO_2 conversion process decreased compared to an electrochemical system (energy efficiency of 5.2% and 1.4% for PEC and electrochemical system, respectively) However, further efforts are still required to improve the overall process performance. This work, therefore, focuses on the preparation, characterization, and evaluation of TiO_2 nanoparticles synthesized in supercritical medium (SC-TiO_2) for the continuous photoelectrochemical conversion of CO_2 in an illuminated photoanode-driven filter-press reactor. The performance of the novel light-responsive materials is analyzed in terms of production rate (*r*), Faradaic efficiency (*FE*), energy efficiency (*EE*), and solar-to-fuel (*STF*) efficiency. The results are compared with the behavior of TiO_2-P25 surfaces in the same reactor configuration to demonstrate the potential applicability of supercritical fluid-based methods for the synthesis of photoactive materials with improved properties. The novelty of the present work lays on: i) CO_2 supplied as gas in the cathode (together with a liquid catholyte), measuring gas-phase chemicals (e.g., C_2H_4) and thus closing all products produced; ii) TiO_2 nanoparticles are synthesized in supercritical medium to improve the properties of benchmark TiO_2-P25, namely BET surface area, light absorption, optical bandgap, or crystallinity; and iii) the use of a membrane electrode assembly (MEA) configuration by coupling the membrane to the photoanode surface, acting as a separator of the PEC cell compartments, for an improved mass/ion/electron transport in the PEC system, thus decreasing the internal cell resistance.

All in all, this work represents a step forward in the development of photoanode-driven PEC systems for a more efficient transformation of CO_2 in continuous mode.

2. Materials and methods

2.1. Synthesis and characterization of SC-TiO_2 nanoparticles

The synthesis of TiO_2 nanoparticles in supercritical CO_2 was performed in an ad hoc designed experimental set-up, which has been described in detail elsewhere [43]. In brief, a thermostatic bath, a high-pressure pump, and a high-pressure synthesis reactor represent the main core of the setup. The powder was obtained by thermal hydrolysis of titanium isopropoxide (TTIP; precursor) with ethanol using supercritical CO_2 as the reaction medium. The synthesis conditions were 20 MPa pressure, 300 ºC temperature, 28 mmol precursor/mmol alcohol molar ratio, and reaction time of 2 h. After the synthesis procedure, solids obtained were removed from the reactor and dried at 105 ºC for 12 h. The solids were then calcinated at 400 ºC for 6 h to remove C pollution and to increase TiO_2 crystallinity. The prepared photoactive materials were comprehensively characterized by several techniques in a previous work [43], namely scanning electron microscopy (SEM), X-ray diffraction (XRD), BET analyses, and Fourier transform infrared (FTIR) spectroscopy. A Cary 6000i Spectrometer equipped with an integrating sphere for powder samples was used for diffuse reflectance spectroscopy (DRS) measurements in the UV-Vis-NIR range, and an Edinburgh Instruments FLSP 920 double grating fluorometer equipped with a Xe lamp and Hamamatsu R928 photomultiplier tube, allowed complementing the characterization with photoluminescence (PL) analyses (emission and excitation) to study the optical properties of both SC-TiO_2 and TiO_2-P25 (dry powder).

2.2. Photoanode preparation and characterization

The light-responsive SC-TiO_2 photoanodes are manufactured by an air-brushing method [21,25]. In brief, SC-TiO_2–based catalytic inks are homogenously deposited over the surface of porous Toray carbon paper (TGP-H-60). The catalytic ink is composed of a mixture of the synthesized SC-TiO_2 photocatalyst, a Nafion® solution (Alfa Aesar, 5 wt%, copolymer polytetrafluoroethylene) as a binder, and isopropanol (Sigma Aldrich, 99.5%) as a vehicle, with a 70:30 SC-TiO_2/Nafion mass ratio and a 3 wt% of total solids (photocatalyst + Nafion) in the isopropanol dispersion. The obtained dispersion is sonicated for at least 30 min to obtain a homogeneous slurry that is subsequently airbrushed on the surface of the carbon paper support. The airbrushing process is carried out at 100 ºC to ensure the complete evaporation of the solvent. The photoactive surfaces are prepared by simple accumulation of layers, reaching a final photocatalytic loading of 3 mg cm^{-2} (experimentally determined by continuous weighing), which is selected based on previous findings [25]. A Nafion® 117 membrane, previously activated in HCl solution for 30 min and rinsed with deionized water, is finally coupled with the prepared photoanode to obtain a photoactive MEA.

The PEC properties of the photoanodes are firstly characterized by linear sweep voltammetry (LSV) with and without LED light illumination when CO_2 is continuously fed into the reactor. Moreover, the prepared light-responsive surfaces are characterized by XRD (Phillips X'Pert MDP X-ray powder diffractometer) before and after 150 min of continuous operation under light irradiation in the photoanode-driven PEC reactor to determine the composition and crystallinity of the photocatalysts.

2.3. PEC cell description and experimental conditions

The light-responsive photoanodes (10 cm^2) are tested at ambient conditions in a commercial filter-press cell reactor (Electrocell A/S), that is adapted to be illuminated with cold UV LED lights (365 nm; 100 mW cm^{-2}) in the anodic compartment, as displayed in Fig. 1. The light intensity is measured by a radiometer (Photoradiometer Delta OMH) and controlled by adjusting the LED intensity and the distance between the microreactor and the LED. The photoanode/dark cathode configuration consists of an illuminated SC-TiO_2/carbon paper as the photoanode, a Cu plate as the dark cathode, and a thin leak-free Ag/AgCl (1 mm) as the reference electrode. The Cu plate is cleaned before each experiment with a HCl solution (37%) to ensure a Cu(0)-based surface [51].

The cell compartments are separated by the MEA (SC-TiO_2 photoanode + Nafion® 117 membrane). Both catholyte and analyte aqueous solutions (1 M KOH) are continuously fed to the reactor through two independent peristaltic pumps at flow rates of 10 mL min^{-1}, whereas a constant gas CO_2 feed (180 mL min^{-1}) is introduced into the cathodic compartment of the PEC cell. Finally, a potentiostat (AutoLabPGSTAT 302N) is used to control the applied potential (E) and measure the generated current density (j). A detailed description of both the experimental setup and the PEC cell configuration can be seen in Fig. 2.

The photoelectrochemical CO_2 reduction tests are carried out by duplicate in continuous mode for 50 min, when a pseudo-stable performance is reached. Besides, the behavior of the photoanodes is investigated during three consecutive runs of 50 min under on/off UV irradiation.

Gas and liquid samples are measured at the reactor outlet (cathode side) every 10 min to calculate the concentration of products obtained in each experiment. A gas chromatograph (GCMSQP2010 Ultra, Shimadzu) equipped with a flame ionization detector (GC-FID) is used to measure the formation of liquid products (i.e., alcohols). The production of formate in the liquid phase is also analyzed with ion chromatography (IC, Dionex ICS 1100). Moreover, gaseous samples are taken and measured using an online gas microchromatograph (3000 Micro GC, Inficon). The concentration results that are two times lower/higher than the average value are discarded (experimental error of $< 16.1\%$) to calculate the following figures of merit:

i) the formation rate for each product per unit of area and time, r (μmol m^{-2} s^{-1});

ii) the Faradaic efficiency (FE), which indicates the selectivity of the reaction towards each product, calculated according to Eq. (1):

$$FE(\%) = \frac{z\,n\,F}{q} \text{x} 100, \tag{1}$$

where z is the theoretical number of electrons exchanged to form the target product, n is the number of moles produced, F represents the Faraday constant (96485 C mol^{-1}), and q is the total charge (C) applied in the process. The concentration of products is normalized to the reacting CO_2 (inlet-outlet) in the system and adjusted to close the balance of products in the photoelectrochemical system;

iii) the energy efficiency (EE), defined as the total energy used towards the formation of the desired product, calculated according to Eq. (2):

$$EE(\%) = \frac{E_T}{E} \text{x} FE, \tag{2}$$

where E is the external (experimentally) applied potential and E_T represents the theoretical voltage needed for the formation of each product. The theoretical potentials for C_2H_4 and CH_3OH (V vs. Ag/AgCl at pH 7) are $-$ 0.539 V and $-$ 0.589 V, respectively [52];

iv) the solar-to-fuel (STF) parameter, which represents the efficiency of the process to produce valuable products with light. In PEC approaches, STF takes into account not only the input power from light irradiation but also the input electrical power (applied voltage – external bias). STF can be calculated as follows:

$$STF = \frac{P_{f,o} + P_{e,o}}{P_s + P_{e,i}} = \frac{A \cdot J_{op} \cdot E_{f,o} \cdot FE}{P_s + P_{e,i}}, \tag{3}$$

where $P_{f,o}$ is the output power contained in the chemical fuel (W), $P_{e,o}$ the output power in the form of electricity (W), P_s the input power from solar irradiation (W), and $P_{e,i}$ the external input electrical power (W).

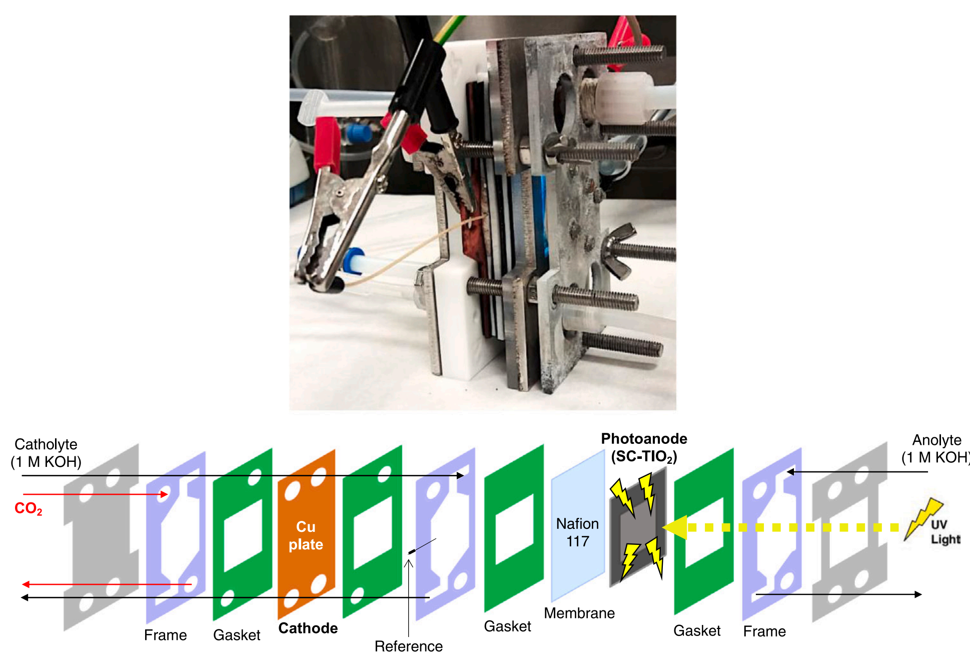

Fig. 1. Illuminated filter-press PEC reactor (above) and graphical illustration of the internal cell components (below).

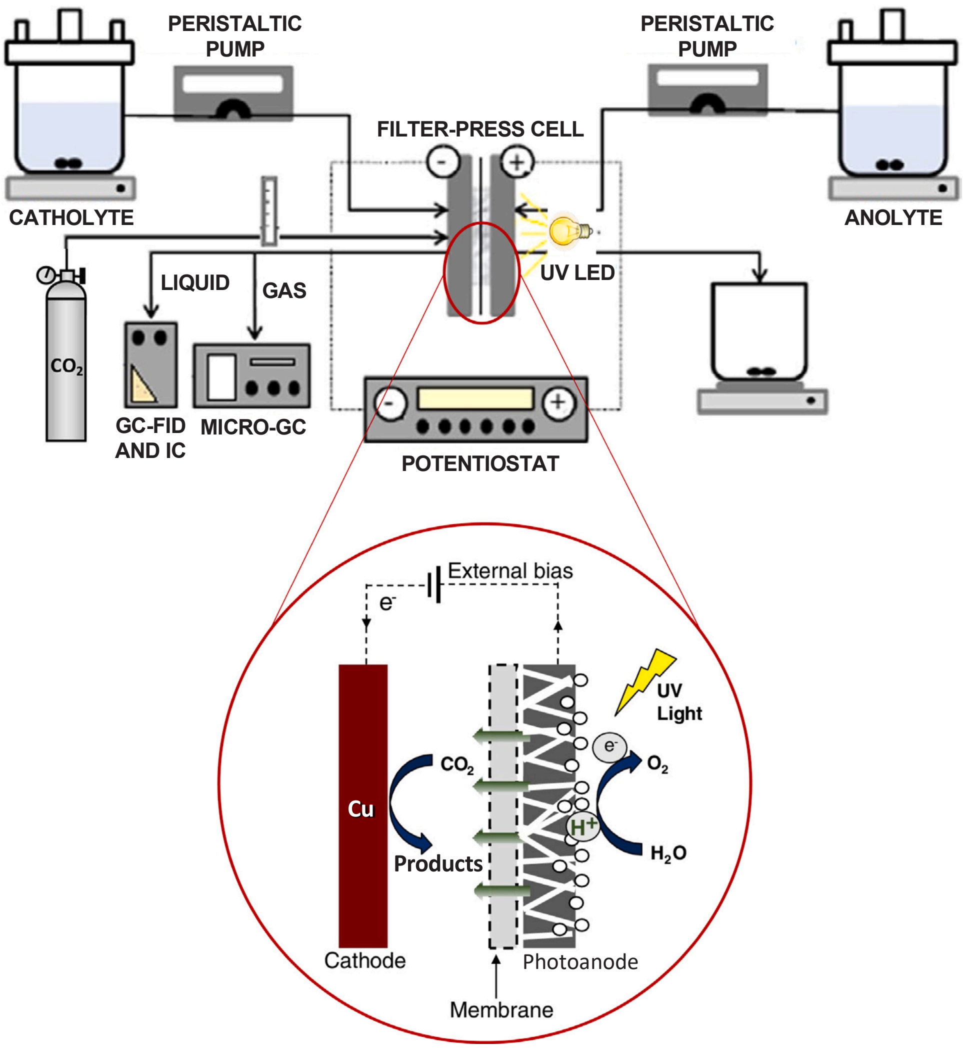

Fig. 2. Experimental system for the continuous PEC conversion of CO_2 including a schematic representation of the photoanode (MEA)/dark cathode configuration. Adapted from [25].

Besides, A represents the geometric area (cm^2), J_{op} the operating current density (A cm^{-2}), $E_{f,o}$ the potential difference (V) between the two half-reactions (i.e., CO_2 reduction product and O_2 from water oxidation) and FE is the Faradaic efficiency.

3. Results and discussion

3.1. Optical properties

The optical properties of the nanoparticles are investigated through DRS and PL analyses, as displayed in Fig. 3. The results show significant differences in reflectance between SC-TiO_2 and commercial TiO_2-P25, as given in the differential spectrum. In particular, the main differences occur under 400 nm, where TiO_2-P25 starts its absorption front (please see DRS of TiO_2-P25 powder as a reference). Both samples show analogous PL spectra at energies below the gap (luminescence maximum: 460 nm), with comparable photoluminescence lifetime for such a blue emission. Nevertheless, their excitation spectroscopy at $\lambda_{max} = 460$ nm is dissimilar. Interestingly, SC-TIO_2 emits for excitation below the P25 gap, peaking at an excitation wavelength around 400 nm (Fig. 3, inset). This implies the existence of low energy states at these energies and a large effective redshift of the gap, of nearly 0.5 eV, in agreement with the absorption spectrum. The comparable luminescence suggests that the emitting traps are similar in nature, and can also be populated upon UV excitation. At 365 nm, SC-TiO_2 shows a factor 1.5 higher extinction. In short, the larger decreased gap energy and optical lower-lying states for SC-TiO_2 allow the creation of excitations at much lower energies. This may contribute to reduce the external bias of the process (and thus the overall energy efficiency) in the presence of light, in contrast with the behavior of commercial TiO_2-P25 photocatalysts.

3.2. PEC characterization

The current densities reached in the filter-press PEC cell as a function of the applied potential (from −1.2 to −2 V vs. Ag/AgCl) and UV light illumination when CO_2 is continuously bubbled into the reactor are displayed in Fig. 4a. As expected, the differences in current density between dark and illuminated conditions become more relevant as the applied voltage increases, owing to a stronger band bending effect that leads to a more efficient charge separation upon light absorption [53, 54]. The current density gap observed represents the highest attainable photocurrent in the PEC system, with a maximum gap of 8.5 mA cm^{-2} at − 2 V vs Ag/AgCl (j_{UV} = 21.6 mA cm^{-2}; j_{dark} = 13.1 mA cm^{-2}). This result represents a two-fold improvement in comparison with commercial TiO_2-P25 photoanodes (current increase: 4.3 mA cm^{-2} [25]) at the same potential level. The current density achieved is comparable (and usually higher) with those results reported so far in TiO_2-based photoanode-driven PEC systems for CO_2 conversion. For example,

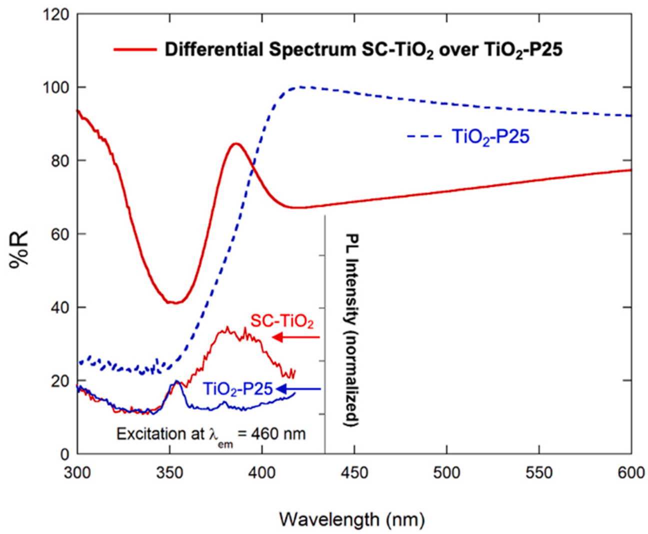

Fig. 3. Differential reflectance spectrum taken for SC-TiO_2 with TiO_2-P25 as the reference signal (DRS for TiO_2-P25 as a blue dotted line). Inset: PL excitation spectra for SC-TiO_2 (red) and TiO_2-P25 (blue) dry powder. The photoexcitation spectra are taken at 460 nm emission. (For interpretation of the references to colour in this figure legend, the reader is referred to the web version of this article).

Yamamoto et al. reported a current density of 2.4 mA cm^{-2} using TiO_2 nanotube photoanodes (6 cm^2) and a metal dark cathode (Pb or Ag) in a divided H-type PEC cell with a methanol-based electrolyte [55]. Similarly, Cheng et al. reported an increased current density (14 mA cm^{-2}) using the same PEC reactor setup with a TiO_2 nanotube photoanode and a Cu foam combined with Pt-modified graphene oxide (Pt-RGO) cathode, with a photoanode/cathode area ratio of 6/1 [38]. More recently, a TiO_2 photoanode and a gas diffusion electrode (GDE) cathode configuration led to a photocurrent density of 1.27 mA cm^{-2} with a low cell voltage bias of 0.8 V [32], whereas higher current densities (9 mA cm^{-2}) have been reported using TiO_2 nanotube arrays (7 cm^2) in a photoanode-driven PEC cell [56]. The values from this work (21.6 mA cm^{-2} with a photocurrent gap of 8.5 mA cm^{-2} at −2 V, and 12.31 mA cm^{-2} with a gap of 4.81 mA cm^2 at −1.8 V) may thus demonstrate the potential of the SC-TiO_2 photoanodes developed.

Besides, the current density evolution over SC-TiO_2 and TiO_2-P25 photoanodes at constant voltage (−1.8 V vs. Ag/AgCl) is shown in Fig. 4b. It should be noted that a potential of − 2 V vs. Ag/AgCl (or more negative) is not considered since it may be undesirable for the production of hydrocarbons [57] and alcohols [58] from CO_2 conversion (due mainly to enhanced H_2 generation), but it might also lead to increased energy consumption, which negatively affects the overall efficiency of the PEC process.

As expected, the illumination of the SC-TiO_2 light-responsive surfaces involves a higher current density (j~12–13 mA cm^{-2}) compared to the same system under dark conditions (j ~ 7.5 mA cm^{-2}). Besides, the

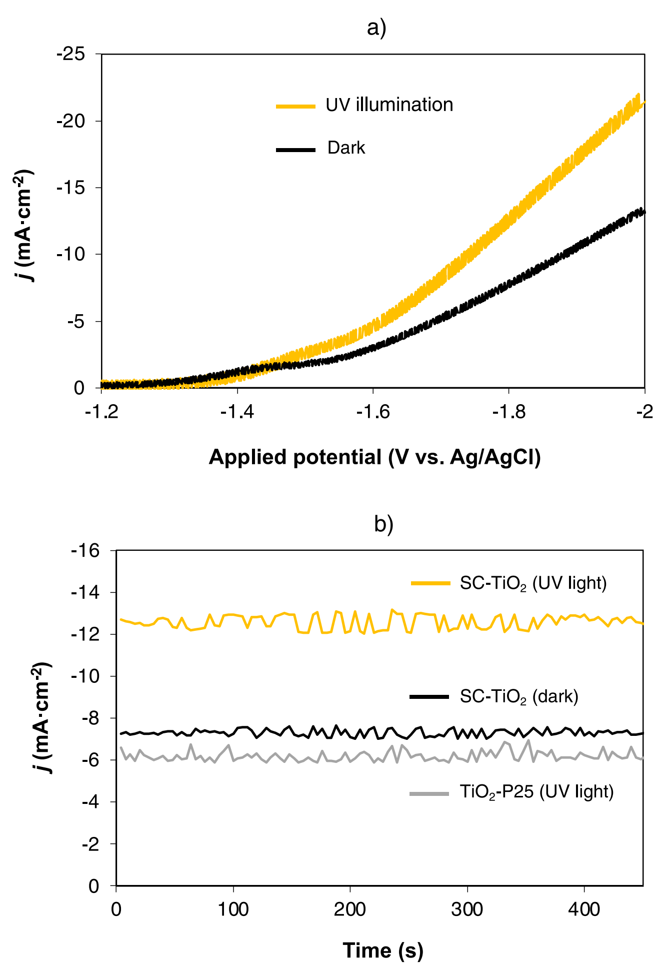

Fig. 4. PEC characterization: a) current-voltage responses of SC-TiO_2 photoanodes with (yellow) and without (black) UV illumination; b) current density evolution at − 1.8 V vs. Ag/AgCl for SC-TiO_2 photoanodes with (yellow) and without (black) LED illumination, compared with TiO_2-P25 photoanodes under illumination (grey). (For interpretation of the references to colour in this figure legend, the reader is referred to the web version of this article).

use of TiO_2-P25 photoanodes leads to significantly decreased current densities in the presence of light ($j \sim 6$ mA cm^{-2}), which proves the enhanced properties of TiO_2 synthesized in supercritical CO_2, such as specific morphology and crystallinity, surface area, light absorption, and optical bandgap energy [43,47]. In particular, the prepared photoactive materials exhibited large surface area than commercial TiO_2-P25 (152 vs. 50 m^2 g^{-1}), as well as a narrow bandgap energy (0.3 eV lower for SC-TiO_2), higher purity (predominant anatase phase), and specific morphology (mixture of particle shapes) [43]. Higher photocatalytic activities are therefore expected for SC-TiO_2 nanoparticles, with easier access of reactant molecules to photoactive sites and a better charge separation and transport.

Then, the stability of the prepared SC-TiO_2 photoanodes is tested under UV light for three consecutive on-off runs of 50 min (Fig. 5). The experiment starts with the UV light on, while the LED lights are turned off at the end of each run (t = 50, 100, 150 min). The analysis shows how the production of CH_3OH, as an example, decays progressively after three consecutive runs. Despite this fact, the increase in CH_3OH yield at the beginning of each run may indicate that the activity loss, partially associated with the blocking of photoactive sites in the photoanode during water oxidation [59], can be mitigated from one on-off cycle to another upon light irradiation. Altogether, pseudo-stable values can be reached at the end of each cycle (4.72, 4.73, and 4.6 μmol m^{-2} s^{-1}, respectively), thus showing a stable PEC conversion of CO_2 under UV light illumination.

To evaluate the composition and crystallinity of the prepared photoactive surfaces, Fig. 6 shows the XRD diffractograms of SC-TiO_2 photoanodes before and after use, including the response of P25-TiO_2 surfaces for comparison. As expected, the XRD response of TiO_2-P25 shows not only peaks related to anatase, but also peaks that can be ascribed to the presence of rutile, since both anatase and rutile are the two main physico-chemically distinct polymorphs in P25 (Sigma-Aldrich, P25). However, the homemade synthesized TiO_2 nanoparticles (SC-TiO_2) exhibit a nearly pure anatase composition, in accordance with previous studies [43,49,60,61]. It should be noted that anatase represents a more photoactive phase than rutile due to surface properties (better response to adsorbates in electron transfer reactions) and solid-state features (improved light absorption and charge transfer) [62], which might lead to an enhanced PEC performance.

Moreover, the diffractograms also reveal that SC-TiO_2 displays higher crystallinity than P25-TiO_2 if we compare the peak height (especially at 25–26º) and resolution of both diffractograms. The results, therefore, show that the calcination process (after synthesis of SC-TiO_2) has been successfully carried out, which should involve more favorable conditions for charge separation [43]. It can be finally noticed that the responses of fresh and used surfaces are very similar, which can be linked to the stability of the system for continuous light-driven PEC operation.

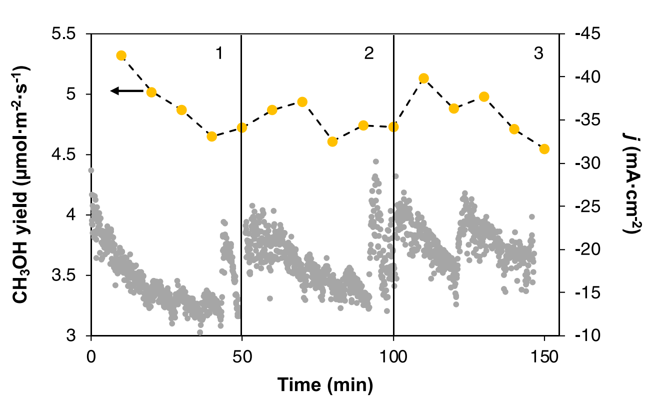

Fig. 5. Time course for the light-driven PEC production of CH_3OH (yellow) and current density (grey) using SC-TiO_2 photoanodes in three consecutive runs (−1.8 V vs. Ag/AgCl).

3.3. Product distribution and process efficiency in PEC cell

The effect of UV light irradiation on the continuous performance of the PEC cell including the SC-TiO_2 photoanodes is studied at constant voltage (−1.8 V vs. Ag/AgCl). The products obtained from CO_2 conversion in the outlet stream are C_2H_4 in the gas phase (with traces of CO) and CH_3OH (with small quantities of C_2H_5OH) in the liquid phase.

The formation rates (r) obtained as a function of light conditions (UV illumination or dark mode) are presented in Table 1. As can be seen, the performance of the UV illuminated PEC system is not only improved in terms of current density (current gap: 5.1 mA cm^{-2}) but also reaction selectivity. Specifically, the increase in current under UV light allows a six-fold enhanced production of C_2H_4 (147.4 vs. 24.2 μmol m^{-2} s^{-1}) and allows the formation of CH_3OH (4.72 μmol m^{-2} s^{-1}), which might be explained by the specific optical properties of SC-TiO_2 photocatalysts (light absorption) and their specific morphology and crystallinity for an enhanced charge separation and transfer in the presence of light [43]. As a result, a high number of electrons (migrating from the photoanode towards the cathode) might be available to proceed with the continuous PEC conversion of CO_2. The production of H_2 also becomes more relevant at higher current densities.

The production rates presented in Table 1 are also normalized by the total charge, q (C), to properly evaluate the activity and selectivity of the process. Interestingly, the production of C_2H_4 is significantly enhanced in the presence of light regardless of the total charge passed through the system during 50 min of continuous PEC operation (0.4 μmol m^{-2} s^{-1} C^{-1} vs 0.11 μmol m^{-2} s^{-1} C^{-1}), which denotes that the selectivity of the reaction is altered at higher current densities (UV illumination).

Similar trends can be seen for *FE* (Fig. 7). The formation of C_2H_4 is improved and the generation of alcohols (i.e., CH_3OH) can be seen. The change in reaction selectivity towards C_2H_4 (*FE* C_2H_4 from 38.2% to 46.6%) and CH_3OH (*FE* CH_3OH = 15.3%) under light irradiation highlights again the improved CO_2 conversion in the cathode at higher current densities, due to the superior photoactivity of SC-TiO_2 photoanodes under the light (improved charge separation and transfer). This leads to an improved PEC process performance with decreased external bias, which is essential from a practical application viewpoint. Besides, the HER is clearly suppressed under UV light irradiation (*FE* H_2 = 38%) since most of the charge passed seems to be used for the selective formation of C_2H_4 and CH_3OH. In the dark, however, H_2 represents the main product at the reactor outlet (*FE* H_2 = 61.5%).

Finally, Table 2 shows *STF* and *EE*, which are crucial figures of merit to evaluate the overall efficiency of the PEC system. The results obtained in the present study are compared to those achieved using illuminated TiO_2-P25 surfaces in our previous work [25].

The use of illuminated SC-TiO_2 surfaces, in comparison with TiO_2-P25 photoanodes, seems to be beneficial for enhanced charge separation and transfer from the photoanode that leads to an improved generation of C_2H_4 from CO_2 conversion at the cathode. The improved characteristics of the synthesized nanoparticles in supercritical CO_2 (i.e., enhanced morphology and high crystallinity) might lead to more efficient separation of electron-hole pairs (suppressing recombination) [43] as well as an increased current density that leads to a more selective formation of C_2H_4 and CH_3OH from CO_2 at the surface of the Cu plate. The *STF* results for C_2H_4 and CH_3OH are enhanced in comparison with the behavior of illuminated TiO_2-P25 photoactive surfaces (5.4% vs. 3.7% for C_2H_4 and 1.9% vs. 1% for CH_3OH) under the same conditions, which once again denotes the enhanced properties of the SC-TiO_2 photoanodes and the effect of the current density on reaction selectivity (especially at high current levels). This result agrees with the decreased gap observed for SC-TiO_2 by differential reflectance analysis (Fig. 3), which allows the creation of excitations at much lower energies. Besides, as expected, the *EE* results under UV irradiation are improved with respect to the behavior of this material in the dark, due to the increased

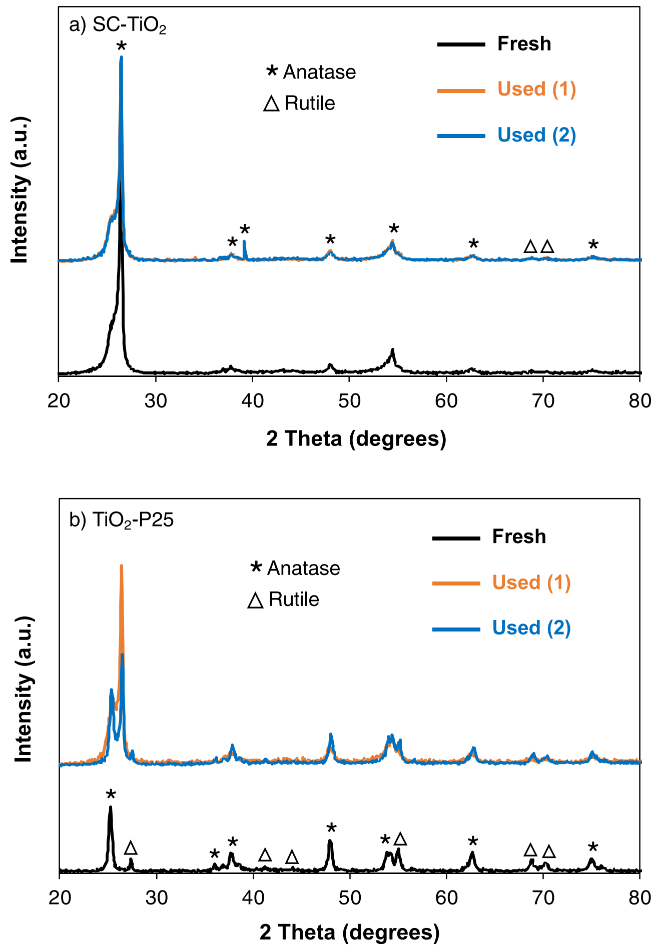

Fig. 6. XRD diffractograms of fresh and used photoactive surfaces: a) SC-TiO_2; b) TiO_2-P25.

Table 1
Production rates (*r*) for CO_2 reduction products and H_2 with and without illumination (−1.8 V vs. Ag/AgCl).

Photoanode	*j* (mA cm^{-2})	*q* (C)	*r* (μmol m^{-2} s^{-1})				*r/q* (μmol m^{-2} s^{-1} C^{-1})
			C_2H_4	C_2H_5OH	CH_3OH	H_2	C_2H_4
SC-TiO_2 (UV illumination)	12.31	369.3	147.4	0.32	4.72	721.5	0.4
SC-TiO_2 (dark)	7.18	215.4	24.2	–	–	233.1	0.11

photocurrent density generated at − 1.8 V vs. Ag/AgCl (Fig. 4a and 4b). The lower *EE* under illumination for C_2H_4 at SC-TiO_2 surfaces (14%) in comparison with the performance of TiO_2-P25 (17.8%) and the invariable *EE* for CH_3OH (5% vs. 5.2%, respectively) can be linked to an increased production of H_2 in the system with SC-TiO_2 photoanodes, due to the higher current density achieved at the cathode.

Fig. 8 shows a schematic representation of the proposed reaction pathways for the generation of C_2H_4 and CH_3OH at the surface of the Cu cathode [63–68].

If we compare the *FEs* obtained for C_2H_4 (as main product) in this work (*FE* C_2H_4 = 46.6%) with other photoanode-driven PEC systems (Table 3), the results outperform the data reported in 1996 when employing a TiO_2 photoanode combined with a Cu-based cathode, where a *FE* C_2H_4 = 24% was obtained, although CH_4 was the main product [69]. Other studies also reported the generation of C_2H_4, as a minor product, in several PEC systems combining different photoanodes and Cu cathodes. For instance, Magesh et al. showed in 2014 a maximum *FE* C_2H_4 = 4.5% for C_2H_4 at WO_3 photoanodes with a Cu cathode [70], whereas this product was not detected when substituting the Cu cathode with Sn/SnO_x electrodes, which indicates the key role of Cu. One year later, the use of a $BiVO_4/WO_3$ photoanode with a Cu cathode led to a *FE* C_2H_4 = 17.7% [71]. Besides, C_2H_4 was a minor product (*FE* C_2H_4 = 2.5%) from CO_2 reduction at a Cu cathode combined with photoanodes based on AlGaN/GaN heterostructures [72].

Thus, the maximum *FE* for C_2H_4 reached in this work is markedly superior to those values reported so far in different photoanode-driven PEC systems, which highlights the relevance of the present study. It should also be mentioned that although a lower *FE* for C_2H_4 was achieved in this work in comparison with our previous study at TiO_2-P25 photoanodes (*FE* C_2H_4 = 59.3%), the *STF* is nevertheless clearly superior due to an increased current density (two-fold improved) at the same potential level, thus demonstrating a more efficient PEC CO_2-to-C_2H_4 process.

Overall, this work represents a step forward into developing more effective PEC systems for CO_2 conversion in continuous mode, which may be helpful to get closer to real applications.

4. Conclusions

In this work, TiO_2 nanoparticles synthesized in supercritical medium

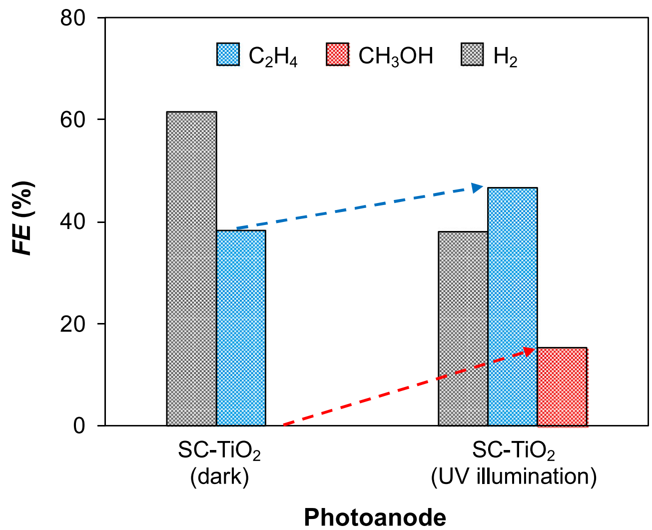

Fig. 7. *FE* results with SC-TiO_2 photoanodes with/without UV illumination (−1.8 V vs. Ag/AgCl).

Table 2
STF and *EE* for CO_2 reduction in the PEC system (−1.8 V vs. Ag/AgCl).

Photoanode	*j* (mA cm^{-2})	*STF* (%)		*EE* (%)		Ref.
		C_2H_4	CH_3OH	C_2H_4	CH_3OH	
SC-TiO_2 (UV illumination)	12.31	5.4	1.9	14	5	This work
SC-TiO_2 (dark)	7.18	–	–	11.5	–	This work
TiO_2-P25 (UV illumination)	5.9	3.7	1	17.8	5.2	[25]

(SC-TiO_2), with a nearly pure anatase composition and improved crystallinity, are investigated in a photoanode-driven photoelectrochemical filter-press reactor for a more efficient transformation of CO_2 into value-added products (i.e., ethylene and methanol) in continuous mode.

The characterization of the photoanodes shows that photocurrent density is higher than most of the values reported in similar photoelectrocatalytic systems and significantly superior (12.31 mA cm^{-2}) than the system in the dark (7.18 mA cm^{-2}). This current level is also higher than that reached with commercial TiO_2-P25 electrodes (5.9 mA cm^{-2}) under the same conditions. The greater decreased gap for SC-TiO_2 observed in differential absorption analyses allows the creation of excitations at much lower energies, which might be responsible for enhancing light-driven process performance.

As a result, the production of ethylene from CO_2 is six-fold improved (147.4 µmol m^{-2} s^{-1}) when using SC-TiO_2 surfaces as photoanodes in comparison with the process performance in the dark. The formation of

Table 3
PEC systems reported for CO_2 conversion to C_2H_4 at Cu-based cathodes in photoanode/dark cathode configurations.

Photoanode	Cathode	Potential and light source	Reaction medium	*FE* (%)	*STF* (%)	Ref.
SC-TiO_2	Cu	-1.8 V vs. Ag/AgCl* UV LED (365 nm)	1 M KOH	46.6	5.4	This work
TiO_2	Cu	-1.8 V vs. Ag/AgCl* UV LED (365 nm)	1 M KOH	59.3	3.7	[25]
TiO_2	Cu/ZnO	Pulsed bias** Sunlight	0.1 M $KHCO_3$	24	–	[69]
WO_3	Cu	0.65 V vs. RHE*** Hg lamp (> 420 nm)	0.5 M $KHCO_3$	4.5	–	[70]
$BiVO_4$/ WO_3	Cu	0.4 V vs. RHE*** Hg lamp (> 420 nm)	0.5 M $KHCO_3$	17.7	–	[71]
AlGaN/ GaN	Cu	-1.47 V vs. Ag/AgCl* Xe lamp (365 nm)	3 M KCl	2.5	–	[72]

Notation: * Cathode potential, ** Potential not available, *** Photoanode potential.

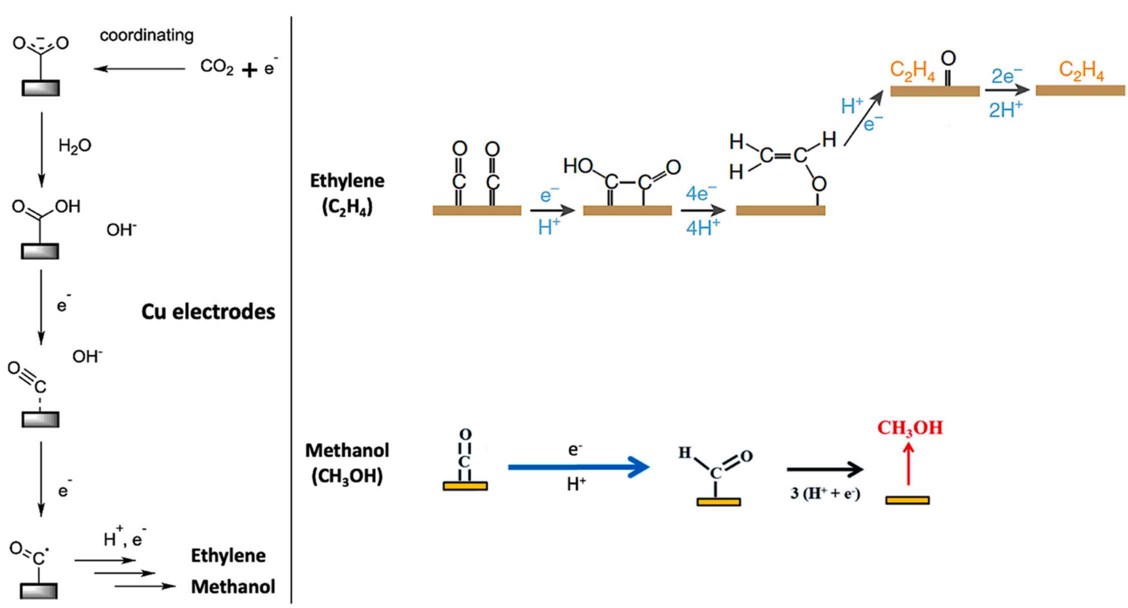

Fig. 8. Reaction mechanisms for the formation of C_2H_4 and CH_3OH from CO_2 at Cu cathodes. Adapted from [63,66,68].

methanol is also favored under illumination (4.72 μmol m^{-2} s^{-1}). Furthermore, the Faradaic efficiencies for both ethylene and methanol (46.6% and 15.3%, respectively) are enhanced under light irradiation, outperforming previous photoanode-driven photoelectrochemical systems reported in the literature. Accordingly, the solar-to-fuel results are improved in the system with illuminated SC-TiO_2 photoactive surfaces (5.4% for ethylene and 1.9% for methanol), in comparison with the behavior of TiO_2-P25 photoanodes (3.7% for ethylene and 1% for methanol).

To sum up, this work reports the continuous light-driven photoelectrochemical conversion of CO_2 using SC-TiO_2photoanodes, promoting a more efficient photoelectrochemical transformation of CO_2 to valuable products.

CRediT authorship contribution statement

Jonathan Albo, Angel Irabien, Rafael Camarillo, Jesusa Rincón, Methodology, Resources, Validation, Supervision, Funding acquisition; **Jonathan Albo, Rafael Camarillo,** Conceptualization; **Ivan Merino-Garcia, Sergio Castro, Jonathan Albo, Ignacio Hernández, Verónica Rodríguez, Rafael Camarillo,** Formal analysis; **Ivan Merino-Garcia, Sergio Castro, Jonathan Albo, Rafael Camarillo, Ignacio Hernández:** Investigation, Roles/Writing – original draft; **Jonathan Albo, Angel Irabien:** Project administration; **Ivan Merino-Garcia, Jonathan Albo, Angel Irabien, Ignacio Hernández, Rafael Camarillo:** Visualization, Writing – review & editing.

Declaration of Competing Interest

The authors declare that they have no known competing financial interests or personal relationships that could have appeared to influence the work reported in this paper.

Acknowledgements

The authors gratefully acknowledge the financial support from Ministerio de Ciencia e Innovación (MCIN), under Ramón y Cajal programme (RYC-2015-17080), and Spanish Ministry of Economy and Competitiveness (MINECO), projects PID2019-104050RA-I00 funded by MCIN/AEI/10.13039/501100011033 and CTQ2016-76231-C2-1-R (MINECO). V.R., R.C., and J.R. wish to thank the Regional Government of Castilla-La Mancha (Project SBPLY/19/180501/000318 and Grants for the training of research personal in public research centers and companies [2016/9989]), as well as the project PID2019-111416RB-I00 funded by MCIN/AEI/10.13039/501100011033. I.H. also acknowledges the funding by the Spanish Ministry of Science, Grant No. MAT2016-80438-P.

References

[1] J. Qiao, Y. Liu, F. Hong, J. Zhang, A review of catalysts for the electroreduction of carbon dioxide to produce low-carbon fuels, Chem. Soc. Rev. 43 (2014) 631–675, https://doi.org/10.1039/c3cs60323g.
[2] W. Zhang, Y. Hu, L. Ma, G. Zhu, Y. Wang, X. Xue, R. Chen, S. Yang, Z. Jin, Progress and perspective of electrocatalytic CO_2 reduction for renewable carbonaceous fuels and chemicals, Adv. Sci. 5 (2018), 1700275, https://doi.org/10.1002/advs.201700275.
[3] E.V. Kondratenko, G. Mul, J. Baltrusaitis, G.O. Larrazábal, J. Pérez-Ramírez, Status and perspectives of CO_2 conversion into fuels and chemicals by catalytic, photocatalytic and electrocatalytic processes, Energy Environ. Sci. 6 (2013) 3112–3135, https://doi.org/10.1039/c3ee41272e.
[4] T. Burdyny, W.A. Smith, CO_2 reduction on gas-diffusion electrodes and why catalytic performance must be assessed at commercially-relevant conditions, Energy Environ. Sci. 12 (2019) 1442–1453, https://doi.org/10.1039/c8ee03134g.
[5] I. Merino-Garcia, L. Tinat, J. Albo, M. Alvarez-Guerra, A. Irabien, O. Durupthy, V. Vivier, C.M. Sánchez-Sánchez, Continuous electroconversion of CO_2 into formate using 2 nm tin oxide nanoparticles, Appl. Catal. B Environ. 297 (2021), 120447, https://doi.org/10.1016/j.apcatb.2021.120447.
[6] A. Sanna, M.R. Hall, M. Maroto-Valer, Post-processing pathways in carbon capture and storage by mineral carbonation (CCSM) towards the introduction of carbon neutral materials, Energy Environ. Sci. 5 (2012) 7781–7796, https://doi.org/10.1039/c2ee03455g.
[7] Y. Zheng, W. Zhang, Y. Li, J. Chen, B. Yu, J. Wang, L. Zhang, J. Zhang, Energy related CO_2 conversion and utilization: advanced materials/nanomaterials, reaction mechanisms and technologies, Nano Energy 40 (2017) 512–539, https://doi.org/10.1016/j.nanoen.2017.08.049.
[8] G.D. Takalkar, R.R. Bhosale, Application of cobalt incorporated Iron oxide catalytic nanoparticles for thermochemical conversion of CO_2, Appl. Surf. Sci. 495 (2019), 143508, https://doi.org/10.1016/j.apsusc.2019.07.250.
[9] I. Merino-Garcia, J. Albo, A. Irabien, Tailoring gas-phase CO_2 electroreduction selectivity to hydrocarbons at Cu nanoparticles, Nanotechnology 29 (2018), 014001, https://doi.org/10.1088/1361-6528/aa994e.
[10] A.A. Al-Omari, Z.H. Yamani, H.L. Nguyen, Electrocatalytic CO_2 reduction: from homogeneous catalysts to heterogeneous-based reticular chemistry, Molecules 23 (2018) 1–12, https://doi.org/10.3390/molecules23112835.
[11] A.U. Pawar, C.W. Kim, M.T. Nguyen-Le, Y.S. Kang, General review on the components and parameters of photoelectrochemical system for CO_2 reduction with in situ analysis, ACS Sustain. Chem. Eng. 7 (2019) 7431–7455, https://doi.org/10.1021/acssuschemeng.8b06303.
[12] P. Chen, Y. Zhang, Y. Zhou, F. Dong, Photoelectrocatalytic carbon dioxide reduction: fundamental, advances and challenges, Nano Mater. Sci. (2021), https://doi.org/10.1016/j.nanoms.2021.05.003.
[13] N. Nandal, S.L. Jain, A review on progress and perspective of molecular catalysis in photoelectrochemical reduction of CO_2, Coord. Chem. Rev. 451 (2022), 214271, https://doi.org/10.1016/j.ccr.2021.214271.
[14] J. Albo, M. Alvarez-Guerra, A. Irabien, Electro-, photo- and-photoelectro-chemical reduction of CO_2, in: Heterogeneous Catalysts: Advanced Design, Characterization and Applications, Wiley-VCH GmbH, 2021, https://doi.org/10.1002/9783527813599.ch36.
[15] K. Li, X. An, K.H. Park, M. Khraisheh, J. Tang, A critical review of CO_2 photoconversion: catalysts and reactors, Catal. Today 224 (2014) 3–12, https://doi.org/10.1016/j.cattod.2013.12.006.
[16] D. Pan, X. Ye, Y. Cao, S. Zhu, X. Chen, M. Chen, D. Zhang, G. Li, Photoanode driven photoelectrocatalytic system for CO_2 reduction to formic acid by using CoOx cathode, Appl. Surf. Sci. 511 (2020), 145497, https://doi.org/10.1016/j.apsusc.2020.145497.
[17] J. Wang, J. Ma, Q. Zhang, Y. Chen, L. Hong, B. Wang, J. Chen, H. Jing, New heterojunctions of CN/TiO2 with different band structure as highly efficient catalysts for artificial photosynthesis, Appl. Catal. B Environ. 285 (2021), 119781, https://doi.org/10.1016/j.apcatb.2020.119781.
[18] A.G. Karthick Raj, C. Murugan, A. Pandikumar, Efficient photoelectrochemical reduction of carbon dioxide into alcohols assisted by photoanode driven water oxidation with gold nanoparticles decorated titania nanotubes, J. CO2 Util. 52 (2021), 101684, https://doi.org/10.1016/j.jcou.2021.101684.
[19] E. Kalamaras, M.M. Maroto-Valer, M. Shao, J. Xuan, H. Wang, Solar carbon fuel via photoelectrochemistry, Catal. Today 317 (2018) 56–75, https://doi.org/10.1016/j.cattod.2018.02.045.
[20] H.J. Yang, H. Yang, Y.H. Hong, P.Y. Zhang, T. Wang, L.N. Chen, F.Y. Zhang, Q. H. Wu, N. Tian, Z.Y. Zhou, S.G. Sun, Promoting ethylene selectivity from CO_2 electroreduction on CuO supported onto CO_2 capture materials, ChemSusChem 11 (2018) 881–887, https://doi.org/10.1002/cssc.201702338.
[21] I. Merino-Garcia, J. Albo, J. Solla-Gullón, V. Montiel, A. Irabien, Cu oxide/ZnO-based surfaces for a selective ethylene production from gas-phase CO_2 electroconversion, J. CO2 Util. 31 (2019) 135–142, https://doi.org/10.1016/j.jcou.2019.03.002.
[22] J. Albo, A. Irabien, Cu2O-loaded gas diffusion electrodes for the continuous electrochemical reduction of CO_2 to methanol, J. Catal. 343 (2016) 232–239, https://doi.org/10.1016/j.jcat.2015.11.014.
[23] J. Albo, M. Alvarez-Guerra, P. Castaño, A. Irabien, Towards the electrochemical conversion of carbon dioxide into methanol, Green Chem. 17 (2015) 2304–2324, https://doi.org/10.1039/c4gc02453b.
[24] W. Zhang, Q. Qin, L. Dai, R. Qin, X. Zhao, X. Chen, D. Ou, J. Chen, T.T. Chuong, B. Wu, N. Zheng, Electrochemical reduction of carbon dioxide to methanol on hierarchical Pd/SnO2 nanosheets with abundant Pd–O–Sn interfaces, Angew. Chem. Int. Ed. 57 (2018) 9475–9479, https://doi.org/10.1002/anie.201804142.
[25] S. Castro, J. Albo, A. Irabien, Continuous conversion of CO_2 to alcohols in a TiO2 photoanode-driven photoelectrochemical system, J. Chem. Technol. Biotechnol. 95 (2020) 1876–1882, https://doi.org/10.1002/jctb.6315.
[26] M. Zhang, J. Cheng, X. Xuan, J. Zhou, K. Cen, CO_2 synergistic reduction in a photoanode-driven photoelectrochemical cell with a Pt-modified TiO2 nanotube photoanode and a Pt reduced graphene oxide electrocathode, ACS Sustain. Chem. Eng. 4 (2016) 6344–6354, https://doi.org/10.1021/acssuschemeng.6b00909.
[27] M.R. Singh, E.L. Clark, A.T. Bell, Effects of electrolyte, catalyst, and membrane composition and operating conditions on the performance of solar-driven electrochemical reduction of carbon dioxide, Phys. Chem. Chem. Phys. 17 (2015) 18924–18936, https://doi.org/10.1039/c5cp03283k.
[28] J.F. de Brito, A.A. da Silva, A.J. Cavalheiro, M.V.B. Zanoni, Evaluation of the parameters affecting the photoelectrocatalytic reduction of CO_2 to CH3OH at Cu/Cu2O electrode, Int. J. Electrochem. Sci. 9 (2014) 5961–5973.
[29] S. Castro, J. Albo, A. Irabien, Photoelectrochemical reactors for CO_2 utilization, ACS Sustain. Chem. Eng. 6 (2018) 15877–15894, https://doi.org/10.1021/acssuschemeng.8b03706.
[30] S. Xie, Q. Zhang, G. Liu, Y. Wang, Photocatalytic and photoelectrocatalytic reduction of CO_2 using heterogeneous catalysts with controlled nanostructures, Chem. Commun. 52 (2016) 35–59, https://doi.org/10.1039/c5cc07613g.

[31] P. Wang, S. Wang, H. Wang, Z. Wu, L. Wang, Recent progress on photo-electrocatalytic reduction of carbon dioxide, Part. Part. Syst. Charact. 35 (2018), 1700371, https://doi.org/10.1002/ppsc.201700371.

[32] K. Kobayashi, S.N. Lou, Y. Takatsuji, T. Haruyama, Y. Shimizu, T. Ohno, Photoelectrochemical reduction of CO_2 using a TiO2 photoanode and a gas diffusion electrode modified with a metal phthalocyanine catalyst, Electrochim. Acta 338 (2020), 135805, https://doi.org/10.1016/j.electacta.2020.135805.

[33] H. Li, Y. Shi, H. Shang, W. Wang, J. Lu, A.A. Zakharov, L. Hultman, R.I.G. Uhrberg, M. Syväjärvi, R. Yakimova, L. Zhang, J. Sun, Atomic-scale tuning of graphene/cubic SiC Schottky junction for stable low-bias photoelectrochemical solar-to-fuel conversion, ACS Nano 14 (2020) 4905–4915, https://doi.org/10.1021/acsnano.0c00986.

[34] J.F. de Brito, C. Genovese, F. Tavella, C. Ampelli, M.V. Boldrin Zanoni, G. Centi, S. Perathoner, CO_2 reduction of hybrid Cu2O–Cu/gas diffusion layer electrodes and their integration in a Cu-based photoelectrocatalytic cell, ChemSusChem 12 (2019) 4274–4284, https://doi.org/10.1002/cssc.201901352.

[35] M. Marszewski, S. Cao, J. Yu, M. Jaroniec, Semiconductor-based photocatalytic CO_2 conversion, Mater. Horiz. 2 (2015) 261–278, https://doi.org/10.1039/c4mh00176a.

[36] S.N. Habisreutinger, L. Schmidt-Mende, J.K. Stolarczyk, Photocatalytic reduction of CO_2 on TiO2 and other semiconductors, Angew. Chem. Int. Ed. 52 (2013) 7372–7408, https://doi.org/10.1002/anie.201207199.

[37] J. Cheng, M. Zhang, G. Wu, X. Wang, J. Zhou, K. Cen, Photoelectrocatalytic reduction of CO_2 into chemicals using Pt-modified reduced graphene oxide combined with Pt-modified TiO2 nanotubes, Environ. Sci. Technol. 48 (2014) 7076–7084, https://doi.org/10.1021/es500364g.

[38] J. Cheng, M. Zhang, J. Liu, J. Zhou, K. Cen, A. Cu, foam cathode used as a Pt-RGO catalyst matrix to improve CO_2 reduction in a photoelectrocatalytic cell with a TiO2 photoanode, J. Mater. Chem. A 3 (2015) 12947–12957, https://doi.org/10.1039/c5ta03026a.

[39] P. Ding, T. Jiang, N. Han, Y. Li, Photocathode engineering for efficient photoelectrochemical CO_2 reduction, Mater. Today Nano 10 (2020), 100077, https://doi.org/10.1016/j.mtnano.2020.100077.

[40] V. Kumaravel, J. Bartlett, S.C. Pillai, Photoelectrochemical conversion of carbon dioxide (CO_2) into fuels and value-added products, ACS Energy Lett. 5 (2020) 486–519, https://doi.org/10.1021/acsenergylett.9b02585.

[41] T.P. Nguyen, D.L.T. Nguyen, V.H. Nguyen, T.H. Le, D.V.N. Vo, Q.T. Trinh, S.R. Bae, S.Y. Chae, S.Y. Kim, Q. Van Le, Recent advances in TiO2-based photocatalysts for reduction of CO_2 to fuels, Nanomaterials 10 (2020) 337, https://doi.org/10.3390/nano10020337.

[42] R. Camarillo, J. Rincón, Photocatalytic discoloration of dyes: relation between effect of operating parameters and dye structure, Chem. Eng. Technol. 34 (2011) 1675–1684, https://doi.org/10.1002/ceat.201100063.

[43] R. Camarillo, S. Tostón, F. Martínez, C. Jiménez, J. Rincón, Preparation of TiO2-based catalysts with supercritical fluid technology: characterization and photocatalytic activity in CO_2 reduction, J. Chem. Technol. Biotechnol. 92 (2017) 1710–1720, https://doi.org/10.1002/jctb.5169.

[44] J.F. de Brito, J.A.L. Perini, S. Perathoner, M.V.B. Zanoni, Turning carbon dioxide into fuel concomitantly to the photoanode-driven process of organic pollutant degradation by photoelectrocatalysis, Electrochim. Acta 306 (2019) 277–284, https://doi.org/10.1016/j.electacta.2019.03.134.

[45] A.G.K. Raj, C. Murugan, P. Rameshkumar, A. Pandikumar, Growth of silver nanodendrites on titania nanotubes array for photoanode driven photoelectrocatalytic reduction of carbon dioxide, Appl. Surf. Sci. Adv. 2 (2020), 100035, https://doi.org/10.1016/j.apsadv.2020.100035.

[46] E. Alonso, I. Montequi, M.J. Cocero, Effect of synthesis conditions on photocatalytic activity of TiO2 powders synthesized in supercritical CO_2, J. Supercrit. Fluids 49 (2009) 233–238, https://doi.org/10.1016/j.supflu.2009.01.005.

[47] J. Jung, M. Perrut, Particle design using supercritical fluids: literature and patent survey, J. Supercrit. Fluids 20 (2001) 179–219. ⟨http://linkinghub.elsevier.com/retrieve/pii/S089684460100064X⟩.

[48] R. Camarillo, S. Tostón, F. Martínez, C. Jiménez, J. Rincón, Enhancing the photocatalytic reduction of CO_2 through engineering of catalysts with high pressure technology: Pd/TiO2 photocatalysts, J. Supercrit. Fluids 123 (2017) 18–27, https://doi.org/10.1016/j.supflu.2016.12.010.

[49] E. Alonso, I. Montequi, S. Lucas, M.J. Cocero, Synthesis of titanium oxide particles in supercritical CO_2: effect of operational variables in the characteristics of the final product, J. Supercrit. Fluids 39 (2007) 453–461, https://doi.org/10.1016/j.supflu.2006.03.006.

[50] B.L. Cushing, V.L. Kolesnichenko, C.J. O'Connor, Recent advances in the liquid-phase syntheses of inorganic nanoparticles, Chem. Rev. 104 (2004) 3893–3946, https://doi.org/10.1021/cr030027b.

[51] J.J. Kim, D.P. Summers, K.W. Frese, Reduction of CO_2 and CO to methane on Cu foil electrodes, J. Electroanal. Chem. Interfacial Electrochem. 245 (1988) 223–244, https://doi.org/10.1016/0022-0728(88)80071-8.

[52] A. Irabien, M. Alvarez-Guerra, J. Albo, A. Dominguez-Ramos, Electrochemical conversion of CO_2 to value-added products, in: Electrochem. Water Wastewater Treat, Elsevier, Amsterdam, 2018, pp. 29–59.

[53] Z. Zhang, J.T. Yates, Band bending in semiconductors: chemical and physical consequences at surfaces and interfaces, Chem. Rev. 112 (2012) 5520–5551, https://doi.org/10.1021/cr3000626.

[54] Y. Hermans, S. Murcia-López, A. Klein, R. Van De Krol, T. Andreu, J.R. Morante, T. Toupance, W. Jaegermann, Analysis of the interfacial characteristics of BiVO4/metal oxide heterostructures and its implication on their junction properties, Phys. Chem. Chem. Phys. 21 (2019) 5086–5096, https://doi.org/10.1039/c8cp07483f.

[55] T. Yamamoto, H. Katsumata, T. Suzuki, S. Kaneco, Photoelectrochemical reduction of CO_2 in methanol with TiO2 photoanode and metal cathode, ECS Trans. 75 (2017) 31–37, https://doi.org/10.1149/07550.0031ecst.

[56] M. Zhang, J. Cheng, X. Xuan, J. Zhou, K. Cen, Pt/graphene aerogel deposited in Cu foam as a 3D binder-free cathode for CO_2 reduction into liquid chemicals in a TiO2 photoanode-driven photoelectrochemical cell, Chem. Eng. J. 322 (2017) 22–32, https://doi.org/10.1016/j.cej.2017.03.126.

[57] I. Merino-Garcia, J. Albo, A. Irabien, Productivity and selectivity of gas-phase CO_2 electroreduction to methane at copper nanoparticle-based electrodes, Energy Technol. 5 (2017) 922–928, https://doi.org/10.1002/ente.201600616.

[58] J. Albo, D. Vallejo, G. Beobide, O. Castillo, P. Castaño, A. Irabien, Copper-based metal–organic porous materials for CO_2 electrocatalytic reduction to alcohols, ChemSusChem 10 (2017) 1100–1109, https://doi.org/10.1002/cssc.201600693.

[59] J. Albo, M.I. Qadir, M. Samperi, J.A. Fernandes, I. de Pedro, J. Dupont, Use of an optofluidic microreactor and Cu nanoparticles synthesized in ionic liquid and embedded in TiO2 for an efficient photoreduction of CO_2 to methanol, Chem. Eng. J. 404 (2021), 126643, https://doi.org/10.1016/j.cej.2020.126643.

[60] Q. Wang, D. Yang, D. Chen, Y. Wang, Z. Jiang, Synthesis of anatase titania-carbon nanotubes nanocomposites with enhanced photocatalytic activity through a nanocoating-hydrothermal process, J. Nanopart. Res. 9 (2007) 1087–1096, https://doi.org/10.1007/s11051-006-9199-x.

[61] Y.C. Wu, Y.C. Tai, Effects of alcohol solvents on anatase TiO2 nanocrystals prepared by microwave-assisted solvothermal method, J. Nanopart. Res. 15 (2013) 1686, https://doi.org/10.1007/s11051-013-1686-2.

[62] M.A. Henderson, A surface science perspective on TiO2 photocatalysis, Surf. Sci. Rep. 66 (2011) 185–297, https://doi.org/10.1016/j.surfrep.2011.01.001.

[63] R. Kortlever, J. Shen, K.J.P. Schouten, F. Calle-Vallejo, M.T.M. Koper, Catalysts and reaction pathways for the electrochemical reduction of carbon dioxide, J. Phys. Chem. Lett. 6 (2015) 4073–4082, https://doi.org/10.1021/acs.jpclett.5b01559.

[64] K.P. Kuhl, E.R. Cave, D.N. Abram, T.F. Jaramillo, New insights into the electrochemical reduction of carbon dioxide on metallic copper surfaces, Energy Environ. Sci. 5 (2012) 7050–7059, https://doi.org/10.1039/c2ee21234j.

[65] A.A. Peterson, F. Abild-Pedersen, F. Studt, J. Rossmeisl, J.K. Nørskov, How copper catalyzes the electroreduction of carbon dioxide into hydrocarbon fuels, Energy Environ. Sci. 3 (2010) 1311–1315, https://doi.org/10.1039/c0ee00071j.

[66] J.P. Jones, G.K.S. Prakash, G.A. Olah, Electrochemical CO_2 reduction: recent advances and current trends, Isr. J. Chem. 54 (2014) 1451–1466, https://doi.org/10.1002/ijch.201400081.

[67] A.J. Garza, A.T. Bell, M. Head-Gordon, Mechanism of CO_2 reduction at copper surfaces: pathways to C2 products, ACS Catal. 8 (2018) 1490–1499, https://doi.org/10.1021/acscatal.7b03477.

[68] D. Ren, J. Fong, B.S. Yeo, The effects of currents and potentials on the selectivities of copper toward carbon dioxide electroreduction, Nat. Commun. 9 (2018) 925, https://doi.org/10.1038/s41467-018-03286-w.

[69] S. Ichikawa, R. Doi, Hydrogen production from water and conversion of carbon dioxide to useful chemicals by room temperature photoelectrocatalysis, Catal. Today 27 (1996) 271–277, https://doi.org/10.1016/0920-5861(95)00198-0.

[70] G. Magesh, E.S. Kim, H.J. Kang, M. Banu, J.Y. Kim, J.H. Kim, J.S. Lee, A versatile photoanode-driven photoelectrochemical system for conversion of CO_2 to fuels with high faradaic efficiencies at low bias potentials, J. Mater. Chem. A 2 (2014) 2044–2049, https://doi.org/10.1039/c3ta14408a.

[71] J.H. Kim, G. Magesh, H.J. Kang, M. Banu, J.H. Kim, J. Lee, J.S. Lee, Carbonate-coordinated cobalt co-catalyzed BiVO4/WO3 composite photoanode tailored for CO_2 reduction to fuels, Nano Energy 15 (2015) 153–163, https://doi.org/10.1016/j.nanoen.2015.04.022.

[72] M. Deguchi, S. Yotsuhashi, H. Hashiba, Y. Yamada, K. Ohkawa, Enhanced capability of photoelectrochemical CO_2 conversion system using an AlGaN/GaN photoelectrode, Jpn. J. Appl. Phys. 52 (2013) 08JF07, https://doi.org/10.7567/JJAP.52.08JF07.